

Weak curvature asymptotics for Debye layers as electrohydrodynamic discontinuities

Philipp G. Marthaler^{*} and Andreas G. Class*Institute for Thermal Energy Technology and Safety, Karlsruhe Institute of Technology, 76131 Karlsruhe, Baden-Württemberg, Germany*

(Received 27 September 2021; accepted 17 February 2022; published 16 March 2022)

Important microfluidic phenomena, such as droplet deformation and cell motion, are impacted by the formation of Debye layers at charged interfaces. Previous studies examined interface problems with leaky dielectrics or the formation of diffuse charge layers. In most cases, the results are derived for weakly curved spherical geometries. Moreover, many studies of streaming-potential phenomena at fluid-solid interfaces lack a macroscale description of effects that are higher than first order. An asymptotic methodology capturing both complex surface geometries and an accurate description of higher-order phenomena is presented in this study. For this purpose, we consider a generic streaming-potential problem. As a result, the complex three-dimensional electrohydrodynamics in the Debye layer are entailed in two-dimensional discontinuity conditions. The latter contain a free parameter, the layer thickness, which mathematically represents the discontinuity position within the Debye layer. It can be used to derive an alternative definition of the Debye thickness capturing the influence of the ζ potential. We introduce a virtual particle whose outer boundary envelopes the solid particle plus a fraction of the Debye layer. It interacts with the macroscopic flow while incorporating the detailed electrohydrodynamics inside the layer.

DOI: [10.1103/PhysRevE.105.035106](https://doi.org/10.1103/PhysRevE.105.035106)

I. INTRODUCTION

The formation of diffuse space-charge (Debye) layers at charged interfaces affects electrolyte flow, charge transport, and causes surface deformation [1]. Those effects are crucial to a class of phenomena ranging from droplet deformation to cell motion. Understanding droplet deformation is imperative for several industrial applications relying on the precise control of the process [2,3]. Significant examples are inkjet printing, spraying of one liquid in another, and droplet pumping. A second field where charged surfaces play an important role is cell biology. One key component of cells is the lipid bilayer membrane acting as an interface to the liquid environment [4]. Vesicles, often used as cell models, are cell-size envelopes consisting of the mentioned bilayer membranes [5]. They are attractive to study as their properties permit a continuum-mechanical description [6] while they mimic various cellular phenomena. In particular, dynamic nonequilibrium phenomena, such as cell breathing or trembling and tumbling, have been subject to theoretical [6–9] and experimental investigations [10,11]. Both mentioned fields are pertinent to the topic of droplet-based microfluidics. In this application, droplets serve as cell models due to the similarity in surface properties between droplet interface bilayers and lipid bilayers. Thus, cell transport and interactions with channels and other cells can be studied, e.g., to develop polymerase chain reaction amplification techniques. Most of the described phenomena appear on droplets or cells of arbitrary shape as illustrated in Fig. 1(a).

Clearly, these important phenomena and their applications have been subject to several investigations. A popular

study addressing the discontinuity of electrical and mechanical properties at a charged fluid-fluid interface is due to Taylor and co-workers [12,13]. They intensively studied liquids with small conductivities: leaky dielectrics. In parallel, other analyses in the field of electrohydrodynamics focused on the behavior of charged particles in electrolytes [14]. Both branches were combined in the seminal analysis by Schnitzer and Yariv [15]. They incorporated ionic transport and the formation of two diffuse charge (Debye) layers in their model. For this purpose, they performed an asymptotic analysis in the double limit of the bilayer interface. As a result, Schnitzer and Yariv [15] derived effective boundary conditions at the interface connecting the outer bulk flow to the convection inside the enveloping boundary. The domain coupling conditions entail the detailed electrohydrodynamic phenomena in the bilayer interface.

In analogy to the fluid-fluid phenomena described above, a spherically shaped streaming-potential problem with a fluid-solid interface [Fig. 1(d)] has been intensively discussed in the literature. In this case, the outer bulk flow disrupts the equilibrium in the Debye layer of dimensionless thickness δ . It thus generates an electric field in the vicinity of the particle surface. The particle behavior and the streaming potential (in this case called sedimentation potential) in this setting were previously examined by a number of authors [16–18]. Similarly to our procedure, several asymptotic approaches [18–21] use δ as an asymptotically small parameter. The focus of these studies lies on the asymptotic correction to Stokes drag considering electroviscous effects. While Cox [18] concluded a correction of $O(\delta^4)$, Yariv *et al.* [21] reestablished the classical result by von Smoluchowski [22] of $O(\delta^2)$. In the present study, we follow the model by Yariv *et al.* [21]. Their approach is based on the assumption that Ohmic charge fluxes in the bulk flow must be balanced by convective charge fluxes in the

^{*}philipp.marthaler@kit.edu

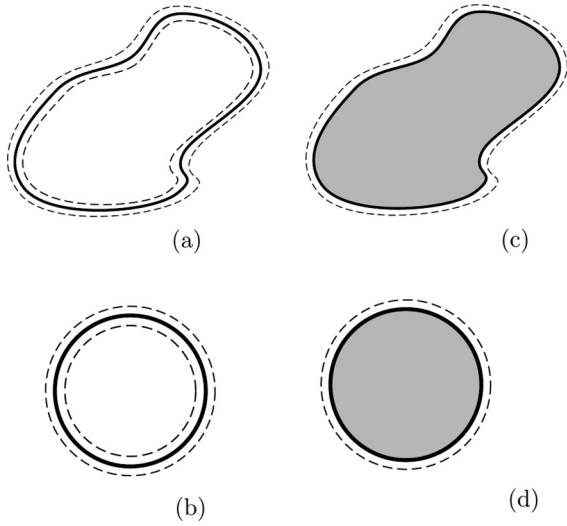


FIG. 1. (a) Liquid-liquid bilayer model, (b) spherical liquid-liquid bilayer model, (c) liquid-solid model, and (d) spherical liquid-solid model.

thin double layer to fulfill charge conservation. Subsequently, they were able to generalize their model for stronger electric fields [23,24].

Yet, most modeling approaches [13,14] and model applications [8,25] focus on a droplet of (nearly) spherical shape as displayed in Figs. 1(b) and 1(d). Performing their analysis in spherical coordinates, Schnitzer and Yariv were able to develop their results in the context of the previous authors' work. However, vesicle and drop shapes are not limited to spherical or ellipsoid geometries. Note that a complex mechanism like cell motion is based on the perpetual deformation of the cell surface [Fig. 1(a)] [26]. Moreover, nonspherical geometries play a role in medical applications, e.g., drug delivery [27].

This work presents a mathematical framework that delivers the conditions for electrical and (fluid-) mechanical discontinuities for nonspherical geometries. In our development, we follow the integral asymptotic procedure first applied by Class *et al.* [28,29]. The basic idea of this approach was recently adapted to electrohydrodynamic phenomena by Marthaler and Class [30] utilizing a set of coupled Stokes and Nernst-Planck equations. In agreement with the previous approaches, the asymptotic method is performed using δ as an asymptotically small parameter.

For the sake of simplicity, we illustrate our approach using a solid-fluid interface problem demonstrated in Fig. 1(c). The conceptual idea and conclusions can be drawn using a problem with a single diffuse layer. Avoiding the double limit of bilayer phenomena is intended to direct focus on the analysis of the tensorial description.

To reach the prescribed goal, we start our analysis with the formulation of surface flows in tensorial notation (compare [31]). We supplement the fluid-dynamic equations to capture electrohydrodynamic phenomena. For this purpose, we consider the generic streaming-potential problem described by Yariv *et al.* [21]. It comprises a charged solid surface which is in contact with a binary and symmetric electrolyte solution. As a result, we obtain a set of coupled equations in tensorial form consisting of the Stokes and

Nernst-Planck equations. Then we perform a distinct treatment of normal and tangential directions to the surface.

In a matched asymptotic expansion, we derive leading-order inner and outer solutions by the asymptotic matching procedure [21,32,33]. The corresponding boundary conditions of the outer solution represent the discontinuity of velocity, pressure, and potential caused by the Debye layer. In the next step, we use the leading-order solution to find discontinuity conditions of higher-order parameters such as stress, mass flux, and electric field. Those usually require asymptotic higher-order solutions, which are impossible or hard to derive with the traditional matching procedure. However, our integral approach delivers those conditions without explicit calculation of the inner solutions. Eventually, this results in two discontinuity conditions for each equation. After deriving our results for arbitrary surfaces, we simplify them for a spherically shaped solid particle [Fig. 1(d)].

For the fluid-fluid phenomena discussed above, those conditions enable domain coupling and yield a closed macroscale description. In the studied fluid-solid case, the discontinuity conditions include a higher-order correction and thus improve accuracy. Moreover, a different perspective can be added: the concept of a *virtual* particle. To form virtual particles, we attribute some fraction of the Debye layer to the particle while the remainder is attributed to the fluid. Depending on the precise location where we place the boundaries of the virtual particle, i.e., where we introduce the mathematical discontinuity, we find corresponding jump conditions. Conceptually, this relates to Prandtl's idea of the description of boundary layers [34,35]. Moreover, the idea of virtual particles has been brought up by Drew *et al.* [36] examining two-phase flow. The outer boundary of the virtual particle coincides with the alternative boundary layer description. It is characterized by surface properties that are different from the solid one.

To address these issues, this article is structured as follows. In Sec. II we set up the governing equations of the problem for generic surface shapes in tensorial notation and derive their solutions. In Sec. III the discontinuity conditions are determined. Definitions of the Debye thickness and the virtual particle are discussed in Sec. IV. The results are shown for the sedimenting spherical particle and discussed in the context of the analysis by Yariv *et al.* [21] in Sec. V. We summarize in Sec. VI.

II. GOVERNING EQUATIONS AND THEIR SOLUTION IN CONTRAVARIANT FORM

A. Dimensionless formulation

We consider a stationary streaming-potential problem as discussed by Yariv *et al.* [21] and displayed in Fig. 2. The numbers mentioned in the following paragraph are typical for a binary aqueous solution with millimolar concentration at room temperature. It is further characterized by the characteristic length scale of the solid r^* (typically $1 \mu\text{m}$), the velocity scale of the bulk flow v_∞ , and the electrolyte properties. In the vicinity of the charged solid an electric double layer exhibiting thickness

$$l_D^* = \sqrt{\frac{\epsilon \epsilon_0^* k_B^* T_a^*}{2 Z^2 e_0^* c_\infty^*}} \quad (1)$$

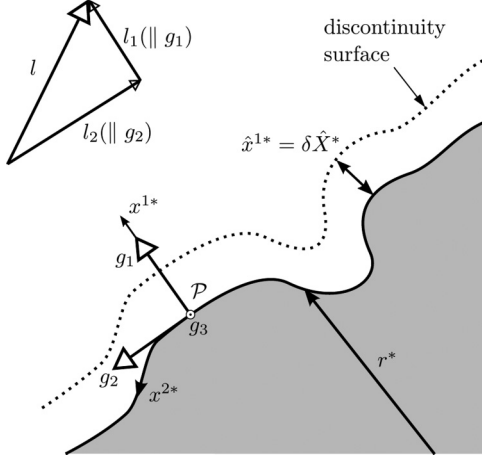


FIG. 2. Generic surface of a solid (gray) with intrinsic length scale r^* with a fluid (white). On each surface point \mathcal{P} , the surface is described by the corresponding base $\{g_1, g_2, g_3\}$. The parallel vector l is invariant in Euclidean space. However, its components vary with \mathcal{P} along the surface and are always parallel to the base vectors $l_i \parallel g_i$ (l_3 component not displayed).

forms. All parameters denoted by $(\dots)^*$ have dimensions, while all other parameters are dimensionless. For a millimolar solution at an ambient temperature $T_a^* = 298$ K, the Debye thickness is typically 10 nm. In the relation above, the vacuum permittivity is denoted by ϵ_0^* , the relative permittivity of water by $\epsilon = 80$, the Boltzmann constant by k_B^* , the valence of both ions by $\mathcal{Z} = 1$, the elementary charge by e_0^* , and the equilibrium charge by c_∞^* . The dimensionless Debye length $\delta = l_D^*/r^* \ll 1$ is utilized as a small parameter for the asymptotic solution of the problem. The solid's surface is exposed to an aqueous solution characterized by the viscosity $\mu^* = 10^{-3}$ Pa s and the diffusion coefficient $D^* = 10^{-9}$ m² s⁻¹. As the electrolyte solution is assumed to be symmetric, diffusion coefficients D_\pm^* for both charges c_\pm^* are equal and the subscript \pm is dropped. The velocity scale is used to define the reference force $\mu^* v_\infty^* r^*$ and stress $\mu^* v_\infty^* / r^*$. The Péclet number $Pe = v_\infty^* r^* / D^*$ is the ratio of convective and charge diffusion fluxes. The electric Hartmann number

$$Ha = \frac{2k_B^* T_a^* r^* c_\infty^*}{\mu v_\infty^*} \quad (2)$$

is defined as ratio of electric and viscous stress scales. The product of both dimensionless numbers is of the order

$$Pe Ha \sim O(\delta^{-2}). \quad (3)$$

The relation is based on the argument that Ohmic charge fluxes in the bulk flow balance convective charge fluxes in the thin double layer (see the Introduction) [21]. The equilibrium concentration c_∞^* serves as the charge scale for the charges c_\pm^* as well as the mean charge concentration $c^* = \frac{1}{2}(c_+^* + c_-^*)$ and the charge density $q^* = \frac{1}{2}(c_+^* - c_-^*)$. The scale for the electric potential is the thermal potential $\phi_{th}^* = k_B^* T_a^* / e^* \sim 25$ mV.

The dimensionless ζ potential $\zeta = \zeta^* / \phi_{th}^*$ is assumed to be constant on the surface. It is of order of the thermal voltage, i.e., $\zeta \sim O(1)$ while $\delta \ll 1$, and thus the Dukhin number becomes vanishingly small. According to Schnitzer

and Yariv [37], surface conduction plays a dominant role for ζ potentials of $\zeta \sim O(\ln \delta)$ and nondilute effects become important for $\zeta \sim O(\delta^{-1})$. For a dimensionless Debye length of $\delta = 0.01$, we expect surface conduction and nondilute effects at voltages of about 0.1 and 1 V, respectively. While the presented approach is limited by these voltages, we refer the reader to authors considering higher Dukhin numbers [37] or steric effects [38] in their work.

B. Geometry of the problem

The described procedure following Class *et al.* [28] and Marthaler and Class [30] is applicable to a wide range of complex-shaped surfaces. Notably, it can be applied to arbitrary surface geometries surrounded by asymptotically thin Debye layers, i.e., we consider $O(\delta)$ curvatures. Details on the used tensor notation can be found in the monograph by Aris [31].

In tensor notation, a coordinate system is characterized by a tensor which in contravariant form reads g^{ij} . The general contravariant metric g^{ij} at each point of the surface is characterized by $g^{1\alpha} = 0$ as the coordinate vector g_1 is always normal to the surface to which the vectors g_α are tangential. The greek indices only represent the two tangential coordinate directions (2,3), while the latin indices include the normal direction (1,2,3). The value $g^{11} = 1$ is chosen without loss of generality. Additionally, we need the volume element \sqrt{g} which is computed from the metric as $\sqrt{g} = (\det g^{ij})^{-1/2}$.

We further introduce a parallel vector l whose direction is arbitrary but invariant with regard to space and time. Yet, the parallel vector can for each surface point be decomposed into different components. Those are parallel to the base vectors and thus also depend on the surface position. To reduce the mathematical complexity of the momentum equation, all of its terms are referred to this parallel vector. The result is a scalar equation that can be dealt with more easily. According to Class *et al.* [28], the normal derivative is $\partial l_1 / \partial x^1 = 0$. Together with the characteristics of the metric $g^{11} = 1$ and $g^{1\alpha} = 0$, we find the corresponding Christoffel symbols of the second kind $\Gamma_{i1}^1 = 0$ and $\Gamma_{11}^1 = 0$. Christoffel symbols result from the derivation of the parallel vector and become

$$\frac{\partial l_i}{\partial x^j} = \Gamma_{ij}^k l_k. \quad (4)$$

C. Generic conservation equation

One of the most generic approaches to physical modeling is the assumption that certain parameters are conserved over a process. An equation representing the conservation of the generic scalar parameter a with the effective three-dimensional (3D) flux $J^j(a)$ and the source term $S(a)$ is in nondimensional form

$$\frac{\partial}{\partial t}(\sqrt{g}a) + \frac{\partial}{\partial x^j}[\sqrt{g}J^j(a)] = \sqrt{g}S(a). \quad (5)$$

The conservation of mass can be found by replacing a with the density ρ^* (here assumed as constant in time and space). Due to the absence of a mass source, we find

$$\frac{\partial}{\partial x^j}(\sqrt{g}v^j) = 0. \quad (6)$$

The Reynolds number is assumed to be small due to the length scale of the particle $r^* \ll 1$ so that transient and convective terms in the momentum equation vanish and the Stokes equation is established [1]. The balance of the Newton and Maxwell stresses

$$\begin{aligned}\sigma^{ij} &= -g^{ij}p + g^{ik}\frac{\partial v^j}{\partial x^k} + g^{kj}\frac{\partial v^i}{\partial x^k} - v^k\frac{\partial g^{ij}}{\partial x^k}, \\ \theta^{ij} &= g^{ik}g^{jl}\frac{\partial \phi}{\partial x^k}\frac{\partial \phi}{\partial x^l} - \frac{1}{2}g^{ij}\frac{\partial \phi}{\partial x^k}\frac{\partial \phi}{\partial x^k}\end{aligned}\quad (7)$$

results in the momentum conservation

$$\frac{\partial}{\partial x^j}[\sqrt{g}(\sigma^{ij} + \theta^{ij})l_i] = 0. \quad (8)$$

The flux term is defined as the product of collective stress $\sigma^{ij} + \theta^{ij}$ and the parallel vector l_i . The latter has the unique feature of vanishing covariant derivatives, i.e., $l_{i,j}$ vanish. The contravariant derivatives, however, do not vanish and include Christoffel symbols of the second kind as mentioned by Class *et al.* [28]. For the equations describing the electrical problem, we choose as scalar parameters ϕ and c_{\pm} and obtain

$$\text{Pe} \frac{\partial}{\partial t}(\sqrt{g}c_{\pm}) + \frac{\partial}{\partial x^j} \left[\sqrt{g} \left(-g^{ij} \frac{\partial c_{\pm}}{\partial x^i} + \text{Pec}_{\pm} v^j \mp c_{\pm} g^{ij} \frac{\partial \phi}{\partial x^i} \right) \right] = 0, \quad \frac{\partial}{\partial x^j} \left(-\delta^2 \sqrt{g} g^{ij} \frac{\partial \phi}{\partial x^i} \right) = \sqrt{g} q. \quad (9)$$

The charge equations are defined by the three fluxes inheriting the phenomena of diffusion $J_{\text{diff}}^j(c_{\pm}) = -g^{ij} \frac{\partial c_{\pm}}{\partial x^i}$, convection $J_{\text{conv}}^j(c_{\pm}) = \text{Pec}_{\pm} v^j$, and electrophoretic charge transport $J_{\text{elph}}^j(c_{\pm}) = \mp c_{\pm} g^{ij} \frac{\partial \phi}{\partial x^i}$. For Poisson's equation describing the electric potential (Gauss's law), we utilize a diffusion-type flux $J^j(\phi) = -\delta^2 g^{ij} \frac{\partial \phi}{\partial x^i}$ and the charge density q as the source of the electric potential.

D. Leading-order solution

We expand all physical parameters $a \in \{v^j, p, \phi, c_{\pm}\}$ and all geometrical parameters $b \in \{\sqrt{g}, g^{ij}, l_i\}$ as a Taylor series

$$\begin{aligned}a &\sim \sum_{n=0} \delta^n a_{(n)}(X, x^{\alpha}, t), \\ b &\sim \sum_{n=0} \frac{\partial^n b(X = \hat{X}, x^{\alpha})}{(\partial x^1)^n} \frac{\delta^n}{n!} X^n \sim \sum_{n=0} \delta^n X^n b_{(n)}(x^{\alpha}).\end{aligned}\quad (10)$$

We note that $v_{(0)}^1 = v_{(1)}^1 = 0$ and $v_{(0)}^{\alpha} = 0$, corresponding to $v^1 \sim O(\delta^2)$ and $v^{\alpha} \sim O(\delta^1)$. As we aim at investigating the limit of flow-driven phenomena, we choose a high Péclet number $\text{Pe} \sim O(\delta^{-2})$ without loss of generality. From Eq. (3) follows $\text{Ha} \sim O(1)$. Also, we introduce the stretched normal coordinate $x^1 = \delta X$ so that all derivatives in the normal direction rise by one order.

By employing the above expansions, coordinate stretch, and assumptions in the governing equations (6)–(9) we find the leading-order equations for the inner problem (parameters denoted by capital letters)

$$\begin{aligned}0 &= \frac{\partial V_{(2)}^1}{\partial X} + \frac{\partial V_{(1)}^{\alpha}}{\partial x^{\alpha}}, \quad 0 = \frac{\partial V_{(1)}^1}{\partial X}, \\ 0 &= -\frac{\partial C_{\pm(0)}}{\partial X} \mp C_{\pm(0)} \frac{\partial \Phi}{\partial X}, \quad 0 = Q_{(0)} + \frac{\partial^2 \Phi_{(0)}}{\partial X \partial X}.\end{aligned}\quad (11)$$

The relevant boundary conditions for the inner flow problem are, according to Yariv *et al.* [21],

$$V^j|_{X=0} = 0, \quad V^j|_{X \rightarrow \infty} \rightarrow v_{\infty}^j, \quad P|_{X \rightarrow \infty} \rightarrow p_{\infty}, \quad (12)$$

and for the electrical problem

$$\begin{aligned}(J_{\text{diff}}^1 + J_{\text{elph}}^1)(C_{\pm})|_{X=0} &= 0, \quad \Phi|_{X=0} = \zeta, \\ C_{\pm}|_{X \rightarrow \infty} &\rightarrow 1, \quad \Phi|_{X \rightarrow \infty} \rightarrow \phi_{\infty}.\end{aligned}\quad (13)$$

For the two latter equations we find the Gouy-Chapman solution [39] for the potential and charges that we write according to Yariv *et al.* using the parameter separation $\Phi_{(0)} = \Psi(X) + \phi_{\infty}(x^{\alpha})$. Van Dyke [33] matching yields

$$\begin{aligned}\Psi &= 2 \ln \frac{1 + \exp(-X) \tanh(\frac{\zeta}{4})}{1 - \exp(-X) \tanh(\frac{\zeta}{4})}, \\ \Psi' &= -2 \sinh \frac{\Psi}{2}, \quad \Psi'' = \sinh \Psi, \\ C_{\pm(0)} &= \exp(\mp \Psi).\end{aligned}\quad (14)$$

The two highest orders are relevant for the flow problem since the leading-order solutions are independent of the electric influence. The solutions are, according to Yariv *et al.*,

$$\begin{aligned}V_{(2)}^1 &= B_{(2)} \frac{X^2}{2}, \quad V_{(1)}^{\alpha} = A_{(1)}^{\alpha} X, \\ V_{(2)}^{\alpha} &= \text{Ha} D_{(2)}^{\alpha} (\zeta - \Psi) + E_{(2)}^{\alpha} \frac{X^2}{2} + F_{(2)} X.\end{aligned}\quad (15)$$

Van Dyke's matching [33] delivers the integration constants

$$\begin{aligned}A_{(1)}^{\alpha} &= \left[\frac{\partial v_{\infty}^{\alpha}}{\partial x^1} \right]_{x^1=0}, \quad B_{(2)} = \left[\frac{\partial p_{\infty}}{\partial x^1} \right]_{x^1=0}, \\ D_{(2)}^{\alpha} &= \left[g^{\alpha\beta} \frac{\partial \phi_{\infty}}{\partial x^{\beta}} \right]_{x^1=0}, \quad E_{(2)}^{\alpha} = \left[g^{\alpha\beta} \frac{\partial p_{\infty}}{\partial x^{\beta}} - 2\gamma \frac{\partial v_{\infty}^{\alpha}}{\partial x^1} \right]_{x^1=0}.\end{aligned}\quad (16)$$

The second-order velocity solution is influenced by the mean curvature γ which appears in the equations via $\frac{\sqrt{g_{(1)}}}{\sqrt{g_{(0)}}} = -2\gamma$ as the ratio of first- and zeroth-order volume elements.

III. DERIVATION OF INTEGRAL DISCONTINUITY CONDITIONS

A. Continuous and discontinuous solutions

We decompose each of the solutions into a continuous and a discontinuous solution using a procedure that differs from the classical approach. The continuous solutions discussed in the preceding section can easily be transformed into the discontinuous solutions. Therefore, we introduce a discontinuity surface that does not necessarily coincide with the particle

surface but can also lie within the fluid. Its position is denoted by $\hat{X}(x^\alpha)$. The discontinuous solution of the basic parameters takes the value of the continuous solution at the wall between the wall and the discontinuity surface. At the discontinuity surface it jumps to the far-field value of the continuous solution. According to Eq. (14), the discontinuous solution for the electric potential is

$$\psi(X, \hat{X}) = \begin{cases} \zeta, & X < \hat{X} \\ 0, & X > \hat{X}. \end{cases} \quad (17)$$

In dependence on that parameter we find the further discontinuous solutions for charges

$$c_{\pm(0)} = \begin{cases} \exp(\mp \zeta), & X < \hat{X} \\ 1, & X > \hat{X} \end{cases} \quad (18)$$

and the flow problem

$$\begin{aligned} v_{(2)}^1 &= B_{(2)} \frac{X^2}{2}, \quad v_{(1)}^\alpha = A_{(1)}^\alpha X, \\ v_{(2)}^\alpha &= E_{(2)}^\alpha \frac{X^2}{2} + F_{(2)} X + \text{Ha} D_{(2)}^\alpha \times \begin{cases} 0, & X < \hat{X} \\ \zeta, & X > \hat{X}. \end{cases} \end{aligned} \quad (19)$$

We note that the continuous and discontinuous solutions for the leading-order velocities are identical. Therefore, we additionally consider the next-order velocity.

Later on, we integrate over both the continuous and discontinuous solutions. We note that all discontinuous solutions are singular at \hat{X} . The integral, however, can still be evaluated by

splitting

$$\begin{aligned} \int_0^\infty \psi dX &= \lim_{\hat{X}_{\text{lim}} \rightarrow \hat{X}} \left(\int_0^{\hat{X}_{\text{lim}}} \zeta dX + \int_{\hat{X}_{\text{lim}}}^\infty 0 dX \right) \\ &= \lim_{\hat{X}_{\text{lim}} \rightarrow \hat{X}} (\zeta \hat{X}_{\text{lim}}) = \zeta \hat{X}. \end{aligned} \quad (20)$$

The derivatives are defined similarly. For the electrical potential, we find $\psi' = 0$ with the same singularity at \hat{X} , which is removable in that case. Thus, integral splitting can be omitted.

B. Idea of integral discontinuity conditions

We are interested in the normal flux discontinuity close to the wall. In the generic conservation equation (5) the fluxes in normal and tangential directions are separated. We derive one equation for the discontinuous model

$$\frac{\partial}{\partial t}(\sqrt{g}a) + \frac{\partial}{\partial x^1}[\sqrt{g}J^1(a)] + \frac{\partial}{\partial x^\alpha}[\sqrt{g}J^\alpha(a)] = \sqrt{g}S(a) \quad (21)$$

and one equation for the continuous model

$$\frac{\partial}{\partial t}(\sqrt{g}A) + \frac{\partial}{\partial x^1}[\sqrt{g}J^1(A)] + \frac{\partial}{\partial x^\alpha}[\sqrt{g}J^\alpha(A)] = \sqrt{g}S(A). \quad (22)$$

As mentioned before, the parameters of the continuous model are denoted by capital letters while the discontinuous model has small parameters. Integrating the difference of both equations over the normal direction x^1 , we receive a formulation for the normal flux discontinuity

$$\int_0^{x_h^1} \frac{\partial}{\partial t}[\sqrt{g}(a - A)] dx^1 + \sqrt{g}[J^1(a)] + \int_0^{x_h^1} \frac{\partial}{\partial x^\alpha} \{ \sqrt{g}[J^\alpha(a) - J^\alpha(A)] \} dx^1 = \int_0^{x_h^1} \sqrt{g}[S(a) - S(A)] dx^1. \quad (23)$$

The normal flux discontinuity is defined as $\llbracket J^1(a) \rrbracket = J^1(a) - J^1(A)$ and the parameter we are mainly interested in. We can manipulate Eq. (23) to find

$$\sqrt{g}\llbracket J^1(a) \rrbracket = \int_0^{x_h^1} \left(-\frac{\partial}{\partial t}[\sqrt{g}(a - A)] - \frac{\partial}{\partial x^\alpha} \{ \sqrt{g}[J^\alpha(a) - J^\alpha(A)] \} + \sqrt{g}[S(a) - S(A)] \right) dx^1. \quad (24)$$

Application of the coordinate stretch $x^1 = \delta X$ results in

$$\sqrt{g}\llbracket J^1(a) \rrbracket = \delta \int_0^\infty \left(-\frac{\partial}{\partial t}[\sqrt{g}(a - A)] - \frac{\partial}{\partial x^\alpha} \{ \sqrt{g}[J^\alpha(a) - J^\alpha(A)] \} + \sqrt{g}[S(a) - S(A)] \right) dX. \quad (25)$$

Using the notation $\llbracket \cdot \rrbracket$ for the discontinuity parameters on the right-hand side as well and expanding all parameters in a Taylor series, we find, for the leading order N ,

$$\sqrt{g_{(0)}}\llbracket J_{(N)}^1(a) \rrbracket = \int_0^\infty \left(-\frac{\partial}{\partial t}(\sqrt{g_{(0)}}\llbracket a_{(N-1)} \rrbracket) - \frac{\partial}{\partial x^\alpha} [\sqrt{g_{(0)}}\llbracket J_{(N-1)}^\alpha(a) \rrbracket] + \sqrt{g_{(0)}}\llbracket S_{(N-1)}(a) \rrbracket \right) dX + O(\delta^{N+1}). \quad (26)$$

The following order(s) can be represented analogously as

$$\sqrt{g_{(0)}}\llbracket J_{(N+1)}^1(a) \rrbracket = \int_0^\infty \left(-\frac{\partial}{\partial t}(\sqrt{g_{(0)}}\llbracket a_{(N)} \rrbracket) - \frac{\partial}{\partial x^\alpha} [\sqrt{g_{(0)}}\llbracket J_{(N)}^\alpha(a) \rrbracket] + \sqrt{g_{(0)}}\llbracket S_{(N)}(a) \rrbracket \right) dX + O(\delta^{N+2}). \quad (27)$$

Yet, this formulation is generic and is valid for any of the governing equations. Therefore, we introduce further simplifications. For any stationary problem the leading-order discontinuity can be written as

$$\sqrt{g_{(0)}}\llbracket J_{(N)}^1(a) \rrbracket = \int_0^\infty \left(-\frac{\partial}{\partial x^\alpha} \{ \sqrt{g_{(0)}}\llbracket J_{(N-1)}^\alpha(a) \rrbracket \} + \sqrt{g_{(0)}}\llbracket S_{(N-1)}(a) \rrbracket \right) dX + O(\delta^{N+1}). \quad (28)$$

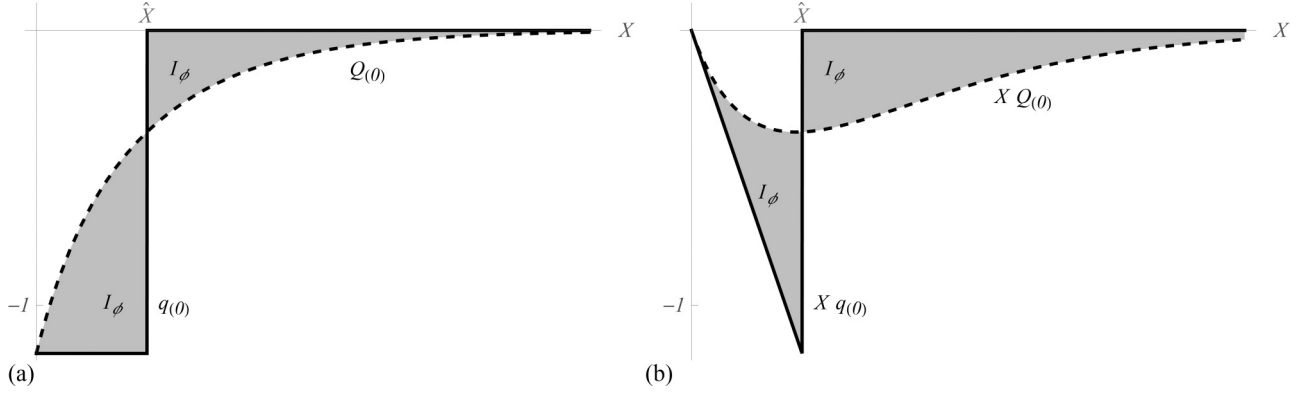


FIG. 3. Illustration of the discontinuity conditions for (a) the electric potential and (b) the charge density equations. The continuous (dashed curve) and discontinuous (solid curve) models coincide at the surface and far from it. The integral jump condition is illustrated by the enclosed area. Only the parts of the solution that depend on X are displayed, i.e., \mathcal{I}_ϕ and \mathcal{I}_q .

We note that our streaming-potential problem is stationary. Moreover, in our set of equations two substantial types occur. A source term only appears in the potential equation. At the same time, the tangential fluxes in the potential equation vanish to lower orders. Thus, the first type of discontinuity formulation evolves as

$$[[J_{(N)}^1(\phi)]] = \int_0^\infty [[S_{(N-1)}(\phi)]] dX. \quad (29)$$

Conversely, the equations for all other parameters $\tilde{a} \in \{v^j, p, c_\pm\}$ lack the source term and therefore only depend on the tangential fluxes. As a result, the discontinuity is

$$[[J_{(N)}^1(\tilde{a})]] = \int_0^\infty \frac{-1}{\sqrt{g_{(0)}}} \frac{\partial}{\partial x^\alpha} \{ \sqrt{g_{(0)}} [[J_{(N-1)}^\alpha(\tilde{a})]] \} dX. \quad (30)$$

For our specific problem, we show the steps in detail for the electric potential and give the solutions for the remaining equations. For the electric potential, the charge density acts as a source term. Substituting this source term for both the discontinuous and the continuous model into Eq. (29), we get

$$\begin{aligned} [[J_{(-1)}^1(\phi)]] &= \int_0^\infty q_{(0)} - Q_{(0)} dX \\ &= \int_0^{\hat{X}} -\sinh \zeta dX + \int_0^\infty \sinh \Psi dX. \end{aligned} \quad (31)$$

Using the relation $\frac{d\Psi}{dX} = -2 \sinh \frac{\Psi}{2}$, we solve the integrals and obtain

$$\begin{aligned} [[J_{(1)}^1(\phi)]] &= -\hat{X} \sinh \zeta + \int_\zeta^0 \frac{\sinh \Psi}{-2 \sinh \frac{\Psi}{2}} d\Psi \\ &= -\hat{X} \sinh \zeta - 2 \sinh \frac{\Psi}{2} \Big|_\zeta^0 \\ &= 2 \sinh \frac{\zeta}{2} - \hat{X} \sinh \zeta =: \mathcal{I}_\phi. \end{aligned} \quad (32)$$

For each of the governing equations we find one discontinuity condition. Those are for the charges

$$[[J_{(0)}^1(q)]] = \text{Pe}_{(-2)} B_{(2)} \mathcal{I}_q, \quad [[J_{(0)}^1(c)]] = \text{Pe}_{(-2)} B_{(2)} \mathcal{I}_c. \quad (33)$$

The integrals \mathcal{I} are specified later in this paragraph. The continuous and discontinuous solutions for both the potential

and charge density equation are displayed in Fig. 3. Depicted are only the terms depending on X as well as the computed integral. The latter is the area between the two curves. The leading-order discontinuities for stress and mass flux in the flow equations are

$$[[J_{(3)}^1(m)]] = \frac{\text{Ha}_{(0)}}{\sqrt{g_{(0)}}} \frac{\partial}{\partial x^\alpha} (\sqrt{g_{(0)}} D_{(2)}^\alpha) \mathcal{I}_m,$$

$$[[J_{(1)}^1[(\sigma^{ij} + \theta^{ij})l_i]]] = -\text{Ha}_{(0)} \gamma \mathcal{I}_{\sigma 1} l_{1(0)}. \quad (34)$$

Later on, we will need the smaller discontinuity for the normal direction

$$[[J_{(2)}^1[(\sigma^{ij} + \theta^{ij})l_i]]] = -\frac{\text{Ha}_{(0)}}{\sqrt{g_{(0)}}} \frac{\partial}{\partial x^\alpha} (\sqrt{g_{(0)}} D_{(2)}^\alpha) \mathcal{I}_{\sigma 2} l_{1(0)}. \quad (35)$$

Yet, we notice that so far no tangential stresses appear. Therefore, we compute, as the next-order discontinuity,

$$[[J_{(3)}^1[(\sigma^{ij} + \theta^{ij})l_i]]] = -\text{Ha}_{(0)} [\tilde{\mathcal{I}}_\sigma l_{1(0)} + f^\alpha (\mathcal{I}_m) l_{\alpha(0)}]. \quad (36)$$

For the stress discontinuity we compute the two highest orders as the normal and tangential parts are of different orders. As the normal part is of $O(\delta^2)$, the part $\tilde{\mathcal{I}}_\sigma$ of $O(\delta^3)$ is of minor interest and not fully evaluated. The corresponding tangential part is defined as

$$f^\alpha (\mathcal{I}_m) = \frac{1}{\sqrt{g_{(0)}}} \frac{\partial}{\partial x^\beta} \mathcal{T}^{\alpha\beta} (D_{(2)} \mathcal{I}_m) + \Gamma_{\beta\gamma(0)}^\alpha \mathcal{T}^{\beta\gamma} (D_{(2)} \mathcal{I}_m), \quad (37)$$

with the tensor $\mathcal{T}^{\alpha\beta}(z) = g^{\alpha\gamma} \frac{\partial z^\beta}{\partial x^\gamma} + g^{\beta\gamma} \frac{\partial z^\alpha}{\partial x^\gamma} - z^\gamma \frac{\partial g^{\alpha\beta}}{\partial x^\gamma}$. The argument can be interpreted as the discontinuity of tangential velocities $\text{Ha}_{(0)}^{-1} \int_0^\infty [[v_{(2)}^\alpha]] dX = D_{(2)}^\alpha \mathcal{I}_m$. We note the analogy of $\mathcal{T}^{\alpha\beta}$ to the Newton stress tensor as defined in Eq. (7). However, we consider only the tangential velocity diffusion here. Accordingly, the result can be interpreted as a viscous stress correction. The function f^α can then be interpreted as the volume force or divergence of that viscous stress correction. The Christoffel symbol of leading order $\Gamma_{\beta\gamma(0)}^\alpha$ results from computing the divergence with respect to the parallel vector. When the velocity discontinuity $[[v_{(2)}^\alpha]]$ or equivalently \mathcal{I}_m becomes zero, the stress correction and the force f^α vanish.

We have separated in the above results the prefactor depending on the tangential coordinates from the integral parts

depending on the normal coordinate X . Those integrals are for the flow parameters

$$\begin{aligned}\mathcal{I}_m &= \mathcal{K}_0(\zeta) + \zeta \hat{X} - \frac{\pi^2}{2}, \quad \mathcal{I}_{\sigma 1} = 4\hat{X} \sinh^2 \frac{\zeta}{2}, \\ \mathcal{I}_{\sigma 2} &= \zeta - 2\hat{X} \sinh \frac{\zeta}{2}\end{aligned}\quad (38)$$

and for the electric parameters

$$\begin{aligned}\mathcal{I}_\phi &= 2 \sinh \frac{\zeta}{2} - \hat{X} \sinh \zeta, \quad \mathcal{I}_q = \zeta - \frac{\hat{X}^2}{2} \sinh \zeta, \\ \mathcal{I}_c &= \frac{\hat{X}^2}{2} \cosh \zeta + \mathcal{M}_1(\zeta) - 4 \ln \cosh \frac{\hat{\Psi}}{4} \\ &\quad + 2\hat{X} \cosh \frac{\hat{\Psi}}{2} + \hat{X} \mathcal{M}_0(\hat{\Psi}) - \mathcal{M}_1(\hat{\Psi}).\end{aligned}\quad (39)$$

In order to make the solutions above easier to read, the abbreviation $\hat{\Psi} = \Psi(\hat{X})$ is used, as well as

$$\begin{aligned}\mathcal{K}_0(\Psi) &= \int \Psi dX \\ &= \Psi[-\ln(1 - e^{-\Psi/2}) + \ln(1 + e^{-\Psi/2})] \\ &\quad - 2 \text{Li}_2(-e^{-\Psi/2}) + 2 \text{Li}_2(e^{-\Psi/2}), \\ \mathcal{M}_0(\Psi) &= \int -\cosh \Psi dX = 2 \cosh \frac{\Psi}{2} + \ln \tanh \frac{\Psi}{4}, \\ \mathcal{M}_1(\Psi) &= \int \mathcal{M}_0(\Psi) dX \\ &= -\frac{1}{2} \left(\ln \tanh \frac{\Psi}{4} \right)^2 - 2 \left(\ln \cosh \frac{\Psi}{2} + \ln \tanh \frac{\Psi}{2} \right).\end{aligned}\quad (40)$$

While we mentioned the jump conditions for the potential and the charge density in [30], we now elaborate on the derivation complemented by the whole set of jump conditions. To obtain the above discontinuity conditions, integrals with respect to the stretched coordinate X have to be solved. Those can be transformed by the relation $\frac{d\Psi}{dX} = -2 \sinh \frac{\Psi}{2}$ and then more elegantly integrated with respect to Ψ .

Finally, we rewrite the discontinuities in Eq. (33) in a more intuitive form. For that reason, we use the gradient, the Laplacian, and the two symbols \parallel and \perp for the directions parallel ($i = \alpha = 2, 3$) and normal ($i = 1$) to the thin layer, respectively. In addition, we employ the integration constants to find, for the hydrodynamic parameters,

$$\begin{aligned}\llbracket v^\perp \rrbracket &= \delta^3 \text{Ha}_{(0)} \nabla_\parallel^2 \phi_\infty \mathcal{I}_m + O(\delta^4), \\ \llbracket \sigma^{\perp\perp} + \theta^{\perp\perp} \rrbracket &= -\delta^1 \text{Ha}_{(0)} \gamma \mathcal{I}_{\sigma 1} - \delta^2 \text{Ha}_{(0)} \nabla_\parallel^2 \phi_\infty (-\zeta) \\ &\quad + O(\delta^3), \\ \llbracket \sigma^{\perp\parallel} + \theta^{\perp\parallel} \rrbracket &= \delta^3 \text{Ha}_{(0)} [-f^\parallel(\mathcal{I}_m)] + O(\delta^4),\end{aligned}\quad (41)$$

and for the electric parameters,

$$\begin{aligned}\llbracket \phi' \rrbracket &= \delta^1 \mathcal{I}_\phi + O(\delta^0), \\ \llbracket J^\perp(q) \rrbracket &= \text{Pe}_{(-2)} \nabla_\perp \phi_\infty \mathcal{I}_q + O(\delta^1), \\ \llbracket J^\perp(c) \rrbracket &= \text{Pe}_{(-2)} \nabla_\perp \phi_\infty \mathcal{I}_c + O(\delta^1).\end{aligned}\quad (42)$$

We note that the discontinuities of mass flow and momentum depend on gradients of the electric field along the surface, similar to the Marangoni effect [40]. In contrast to that, the charge fluxes originate from the electric field perpendicular to the surface.

IV. LAYER THICKNESS AND THE VIRTUAL PARTICLE

The set of discontinuity conditions derived in the preceding section is not uniquely defined. It depends on the layer thickness \hat{X} which behaves as $\lim_{\delta \rightarrow 0} \hat{X} = 0$. While for the first-order solutions the exact position of the discontinuity surface is irrelevant, it becomes significant for the solutions of higher order. In general, the parameter \hat{X} can be chosen freely. For each choice, one consistent set of discontinuity conditions evolves, representing the electrohydrodynamic physics inside the layer.

Although any choice $\hat{X} \geq 0$ is possible, there are some choices that lead to more convenient sets of discontinuity conditions. For instance, the results can be applied much more easily in numerical simulations. Each choice for $\hat{X} > 0$ defines a new particle that includes the solid particle together with a fluid film of thickness \hat{X} . We call that new particle the virtual particle. Its properties differ from those of the solid particle and are specified in the form of the discontinuity conditions.

Simpler properties can be achieved by having one vanishing condition. Each discontinuity condition vanishes if the relevant integral $\mathcal{I} = 0$. This can be illustrated by the condition $\mathcal{I}_m = 0$. Here we find a virtual particle with no excess mass fluxes through the surface. However, the mass flux discontinuity of $O(\delta^3)$ is small enough to be neglected independently of the choice of \hat{X} . Thus, one of the integrals for the electrical problem might be a better choice. Different possibilities are

$$\begin{aligned}0 = \llbracket v^\perp \rrbracket &\Rightarrow \hat{X}_m = \frac{1}{\zeta} \left(\frac{\pi^2}{2} - \mathcal{K}_0(\zeta) \right), \\ 0 = \llbracket \sigma^{\perp\perp} + \theta^{\perp\perp} \rrbracket &\Rightarrow \hat{X}_\sigma = 0, \\ 0 = \llbracket \phi' \rrbracket &\Rightarrow \hat{X}_\phi = \frac{2 \sinh \frac{\zeta}{2}}{\sinh \zeta}, \\ 0 = \llbracket J^\perp(q) \rrbracket &\Rightarrow \hat{X}_q = \sqrt{\frac{2\zeta}{\sinh \zeta}}, \quad 0 = \llbracket J^\perp(c) \rrbracket \Rightarrow \hat{X}_c.\end{aligned}\quad (43)$$

The classical definition of the layer thickness (which was discussed earlier) does not include the ζ potential. However, higher ζ potentials lead to an increase of the polarization and a stronger attraction of charges. The layer becomes thinner as displayed in Fig. 4. All thicknesses \hat{X} capture this phenomenon as

$$\lim_{\zeta \rightarrow \infty} \hat{X}_k = 0 \quad \text{for } k = m, \sigma, \phi, q, c. \quad (44)$$

Figure 4 presents data for $\zeta \in [0, \delta^{-1}]$. For $\zeta \gg O(\delta^{-1})$ nondilute effects appear which are not captured by the described model. In particular, ζ potentials $\zeta \sim O(\ln \delta)$ give rise to surface conduction and higher Dukhin numbers [37]. The model does not hold in that case. The macroscale description

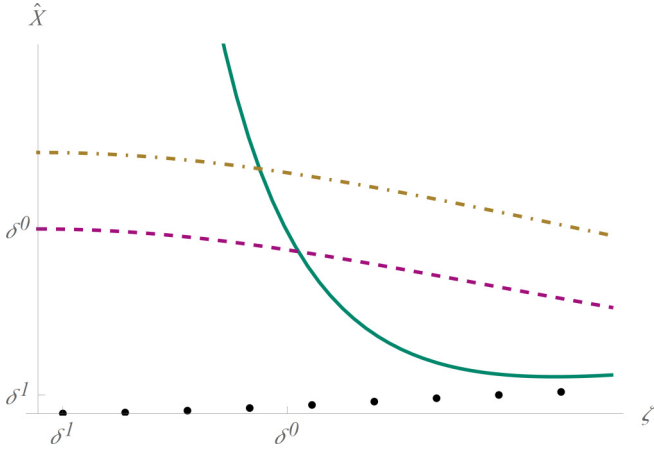


FIG. 4. Layer thickness vs position of the discontinuity surface by different definitions [green solid line, $\hat{X}_m(\zeta)$; magenta dashed line, $\hat{X}_\phi(\zeta)$; and brown dash-dotted line, $\hat{X}_q(\zeta)$]. The black dots represent $\hat{X}_c(\zeta)$, which was computed numerically from $\mathcal{I}_c = 0$. The diagram shows values for $\zeta \in [0, \ln \delta]$.

of our thickness definition is

$$\hat{x}^1 = \delta \hat{X}(\zeta) = \frac{1}{r^*} \sqrt{\frac{\epsilon_0^* \epsilon_r k_B^* T_a^*}{2 \mathcal{Z}^2 e^{*2} c_\infty^*}} \hat{X}(\zeta). \quad (45)$$

The layer becomes thinner for higher ζ potentials and when more charges c_∞^* are in the fluid. In a more complex case with a ζ potential $\zeta(x^\alpha)$ varying along the wall, the layer thickness $\hat{X}(x^\alpha)$ varies as well. In Fig. 4 the layer thickness with respect to the mean salt concentration $\hat{X}_c(\zeta)$ grows with increasing ζ . This results from the formation of an intermediate diffusion layer, which is described in detail by Yariv *et al.* [21].

V. INTEGRAL EFFECTS ON A SEDIMENTING SPHERE

We now apply our results to the specific streaming-potential problem of a sedimenting sphere (Fig. 5). For

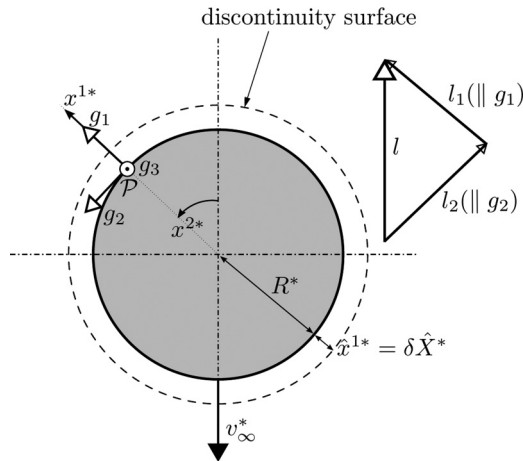


FIG. 5. Problem statement for the sedimenting sphere with radius R^* : definition of the spherical coordinates and the corresponding base vectors. Decomposition of parallel vector l corresponds to coordinates at point \mathcal{P} .

this purpose, we utilize the sedimentation velocity and particle radius as references. As integral effects, like the electrohydrodynamic drag, have been of great interest in the literature [18,19,21], we choose the upward direction (opposite to the velocity) as the direction of interest. We already have our results with regard to the arbitrary parallel vector. Thus, it is convenient to define its direction to coincide with the direction of interest and choose its length to unity.

In this setting, we simplify the coordinates from curvilinear to spherical. The radial coordinate is denoted by x^1 and the polar and azimuthal directions are $x^2 \in [0, 2\pi]$ and $x^3 \in [0, \pi]$, respectively. As a result, we find the metric

$$g^{ij} = \begin{pmatrix} 1 & 0 & 0 \\ 0 & (x^1)^{-2} & 0 \\ 0 & 0 & [(x^1) \sin(x^2)]^{-2} \end{pmatrix} \quad (46)$$

and the volume element

$$\sqrt{g} = \sqrt{g_{(0)}} = (x^1)^2 |\sin(x^2)|. \quad (47)$$

The parallel vector is projected to the spherical base by

$$l_{1(0)} = \cos x^2 l_{(0)}. \quad (48)$$

We find, according to Stokes [41], that the pressure field on the sedimenting sphere is equal to

$$p_\infty = -\frac{3}{2} \cos x^2, \quad (49)$$

and from Yariv *et al.* [21] it follows that

$$\phi_\infty = \text{Pe}_{(-2)} \zeta p_\infty = -\frac{3}{2} \text{Pe}_{(-2)} \zeta \cos x^2. \quad (50)$$

A. Drag correction

Integrating the first-order solutions results in inaccurate second-order solutions. The derived discontinuity conditions serve as corrections in this case. We estimate the influence of our correction by comparing it to the electrohydrodynamic drag that was evaluated by Yariv *et al.* [21].

To reach this goal, we choose the discontinuity coinciding with the particle surface at $\hat{X} = 0$ and integrate over the polar coordinate. The problem is due to its symmetry independent of the azimuthal coordinate. Our result of leading order does not deliver a correction to the electrohydrodynamic drag as its surface integral vanishes. We employ $\hat{X} = 0$ in the correction of $O(\delta^2)$ to find

$$\begin{aligned} & \sqrt{g_{(0)}} \llbracket J_{(2)}^1 ((\sigma^{ij} + \theta^{ij}) l_i) \rrbracket \\ &= -\text{Ha}_{(0)} \delta^2 \frac{\partial}{\partial x^\alpha} \left(\sqrt{g_{(0)}} g_{(0)}^{\alpha\beta} \frac{\partial \phi_\infty}{\partial x^\beta} \right) \left(\zeta - 2\hat{X} \sinh \frac{\zeta}{2} \right) l_{1(0)} \\ &= -3 \text{Ha}_{(0)} \delta^2 \text{Pe}_{(-2)} \zeta \cos x^2 |\sin x^2| \left(\zeta - 2\hat{X} \sinh \frac{\zeta}{2} \right) l_{1(0)}. \end{aligned} \quad (51)$$

We then integrate the flux discontinuity over the surface $\partial\Omega$. From the definition of the fluxes, all discontinuity conditions are directed from the particle to the fluid. As we are interested in the drag on the particle, we evaluate the integral with a

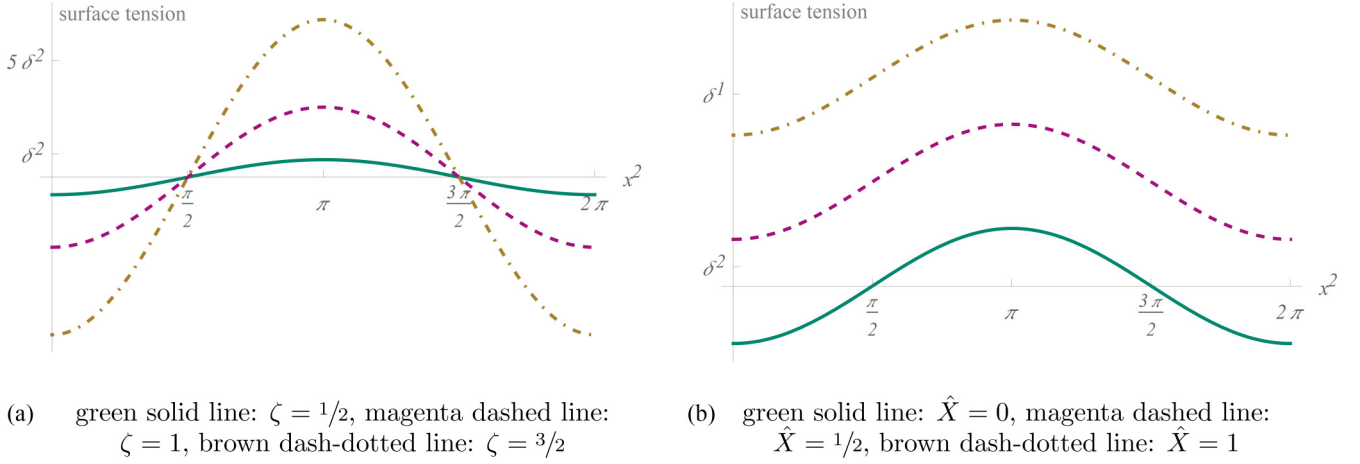


FIG. 6. Surface tension correction over the polar variable x^2 for different (a) ζ potentials and (b) discontinuity conditions \hat{X} .

negative sign to find the force correction

$$\begin{aligned}
 \llbracket \mathcal{F} \rrbracket &= \delta^2 \int_{\partial\Omega} -\llbracket J_{(2)}^1[(\sigma^{ij} + \theta^{ij})l_i] \rrbracket d(\partial\Omega) \\
 &= \delta^2 \int_0^\pi \int_0^{2\pi} -\sqrt{g_{(0)}} \llbracket J_{(2)}^1[(\sigma^{ij} + \theta^{ij})l_i] \rrbracket dx^2 dx^3 \\
 &= 3\pi \text{Ha}_{(0)} \delta^2 \text{Pe}_{(-2)} \zeta^2 \int_0^{2\pi} \cos x^2 |\sin x^2| l_{1(0)} dx^2 \\
 &= 3\pi \text{Ha}_{(0)} \delta^2 \text{Pe}_{(-2)} \zeta^2 \left(\frac{4}{3} l_{(0)} \right) \\
 &= 4\pi \text{Ha}_{(0)} \delta^2 \text{Pe}_{(-2)} \zeta^2 l_{(0)}. \quad (52)
 \end{aligned}$$

We note that this correction is of the same order as von Smoluchowski's basic relation [22] that $\mathcal{F}_{\text{D, Smol}} \sim \zeta^2 l$ and the drag calculated by Yariv *et al.* [21] using their outer solutions and the formula by Brenner [42].

B. Further integral effects

The choice $\hat{X} = 0$ is made in all publications on this topic which are known to the authors [16–18,21]. However, there are several possibilities for \hat{X} in the limit $\delta \rightarrow 0$.

As mentioned before, an intuitive approach is to choose one of the fluxes to vanish and define a virtual particle with $\hat{X} \neq 0$. The normal stress discontinuity depending on both the (constant) ζ and \hat{X} is displayed in Fig. 6. The value of ζ affects the amplitude of the stress discontinuity, while \hat{X} defines the mean value of the periodic distribution. The leading-order effect is an excess surface stress originating from a curved Debye layer. However, the integral value of this effect is zero. The $O(\delta^2)$ surface stress can be described as a Marangoni-type effect as it depends on the tangential electric field $\nabla_\perp \phi_\infty$. Shear stress corrections appear first at $O(\delta^3)$ and are small enough to be neglected.

With increasing ζ the discontinuity position \hat{X} becomes smaller according to Eq. (44). With the observations from before, we find that in that case the amplitudes increase and the mean value over the circumference of the stress discontinuity vanishes. For small ζ the opposite effects can be observed.

Besides the kinematics, the relocation and accumulation of charges is a topic of interest. The flux discontinuity $\llbracket J_{(0)}^1(q) \rrbracket$ and $\llbracket J_{(0)}^1(c) \rrbracket$ describe the excess “sucking in” and “spitting out” of charges into and from the virtual particle. Their integral values

$$\begin{aligned}
 \mathcal{J}_q &= \int_0^\pi \int_0^{2\pi} \sqrt{g_{(0)}} \llbracket J_{(0)}^1(q) \rrbracket dx^2 dx^3 = 0, \\
 \mathcal{J}_c &= \int_0^\pi \int_0^{2\pi} \sqrt{g_{(0)}} \llbracket J_{(0)}^1(c) \rrbracket dx^2 dx^3 = 0 \quad (53)
 \end{aligned}$$

vanish, which means that at each point of time exactly the same amount of charge is transported into and out of the particle. The sedimentation potential is found as

$$\mathcal{J}_\phi = \int_0^\pi \int_0^{2\pi} \sqrt{g_{(0)}} \llbracket J_{(0)}^1(\phi) \rrbracket dx^2 dx^3 = 4\pi \llbracket J_{(0)}^1(\phi) \rrbracket. \quad (54)$$

The parameter $\llbracket J_{(0)}^1(\phi) \rrbracket$ does not depend on the surface coordinates x^α . Therefore, the integral result is the product of the surface area with the flux discontinuity. The particle acts as a source of the electric field.

VI. CONCLUSION

The present study derived from first principles discontinuity conditions of a macroscopic model replacing the Debye layers on arbitrarily shaped surface geometries. These include corrections to the second-order parameters stress, mass flux, charge fluxes, and electric field. In contrast to that, integration of just the first-order parameters, i.e., velocity, pressure, charge, and electric potential, ignores important physical effects that can be captured by our approach. Unlike the leading-order parameters, the correction terms depend on the precise location of the discontinuity surface within the Debye layer. For each surface, which can be arbitrarily chosen, we found one consistent set of such discontinuity conditions which close the corresponding macroscopic problem. These conditions represent a physical simplification, incorporating complex 3D electrohydrodynamics in 2D jumps. For instance, the discontinuities of mass flow and momentum depend on gradients of the electric field along the surface, similar to the Marangoni effect [40].

Although the discontinuity position is a free parameter, it can be used to simplify results. Enforcing that the correction term of one specific conservation equation vanishes, we found for each conservation equation corresponding positions that can be interpreted as definitions for the Debye thickness. Unlike the classical definition, they take the ζ potential into account. At high ζ potentials, ions are strongly attracted to the solid surface, which causes the layer to shrink, while at low ζ potentials the layer becomes wider. This effect was captured by our definitions of the Debye thickness.

Eventually, we defined virtual particles, i.e., particles which comprise not only the solid but also some fraction of the Debye layer. These virtual particles are bounded by the discontinuity surface. The macroscopic outer flow and physics need to be supplemented by a consistent set of boundary conditions, i.e., the derived jump conditions. As the discontinuity surface, i.e., the virtual particle, can be arbitrarily chosen, the consistent jump conditions take into account the exact boundary of the virtual particle. The geometry, i.e., the boundary, can be chosen to be aligned with the aim of the investigation. Note the analogy to the boundary layer thickness definitions by Prandtl [35]. By choosing \hat{X}_m or \hat{X}_σ we found an equivalent to the displacement or momentum loss thickness. In addition, we found distinct thicknesses for the electric problem. In our case, the latter are of higher order and thus more important. In particular, we suggested defining a thickness based on the charge density flux. As charge density is an electric field source, we could avoid perturbations in the electric field around the virtual particle by choosing the mentioned flux to vanish. The ζ potential stays the only source of the electric field.

As indicated in the Introduction, the proposed methodology is applicable beyond streaming potential phenomena with constant surface charge. The complex interplay between variant surface charge and an arbitrary surface is fundamental for cell motion and droplet deformation. While the present study represents a step in this direction, further work should focus on ζ potentials that are functions of space and/or time.

Drag perturbations due to streaming potentials have been widely discussed in the theoretical literature. Yet, the pos-

sibilities of experimental validation are very limited for this specific problem. Therefore, an extension of the proposed model capturing applied electric fields is desirable. For that purpose, an outer electric field can mimic the shape of the surface potential. In fact, due to the controllability of the outer conditions, most experimental settings in this context include an applied field. By controlling its amplitude, significant deviations in the particle movement can be measured for both solid and deformable particles, making the experimental validation of the presented methodology possible.

For a bilayer problem, such as a drop or vesicle, the jump conditions do not describe the parameter variation between the outer solution of the surrounding fluid and the solid particle surface. In a bilayer problem, the discontinuity conditions connect both fluid domains, the one of the surrounding fluid and the one encapsulated drop domain. Despite these differences, for moderate Péclet numbers the leading-order electric problem has strong analogies to the Gouy-Chapman solution. In this work, the electric effects originate from the intrinsic surface charge of the particle, while in bilayer problems the fluid-fluid interface acts as a capacitor. Under the influence of an outer electric field, ions travel to the interface and accumulate, giving rise to excess charges and potentials on both sides of the interface. Due to the interface, the bilayer case is described by a more complex set of equations, including boundary conditions for charge separation and stress continuity as well as one equation describing the interface deformation. By adding the discontinuity position as an additional degree of freedom, it is possible to derive a set of jump conditions without solving the whole inner problem. In numerical simulations, these conditions make a macroscopic solution of the problem possible without a detailed treatment of the 3D electrohydrodynamics inside the layer.

ACKNOWLEDGMENTS

We acknowledge support from the Framatome Professional School. Furthermore, we thank Jorge Yanez for passionate and fruitful discussions.

- [1] J. Happel and H. Brenner, *Low Reynolds Number Hydrodynamics: With Special Applications to Particulate Media* (Springer, The Hague, 1983).
- [2] D. A. Saville, *Annu. Rev. Fluid Mech.* **29**, 27 (1997).
- [3] D. Stefanitsis, G. Strotos, N. Nikolopoulos, E. Kakaras, and M. Gavaises, *Int. J. Heat Fluid Flow* **76**, 274 (2019).
- [4] B. Alberts, A. Johnson, J. Lewis, D. Morgan, M. Raff, K. Roberts, and P. Walter, *Molecular Biology of the Cell*, 6th ed. (Norton & Company, New York, 2014).
- [5] J. T. Schwalbe, P. M. Vlahovska, and M. J. Miksis, *J. Fluid Mech.* **647**, 403 (2010).
- [6] W. Helfrich, *Z. Naturforsch. C* **28**, 693 (1973).
- [7] C. Misbah, *Phys. Rev. Lett.* **96**, 028104 (2006).
- [8] J. T. Schwalbe, P. M. Vlahovska, and M. J. Miksis, *Phys. Rev. E* **83**, 046309 (2011).
- [9] M. Ondrušová and I. Cimrák, in *Proceedings of the 2017 International Conference on Information and Digital Technology, Singapore, 2017* (ACM, New York, 2017), pp. 288–292.
- [10] A. E. Patteson, A. Gopinath, M. Goulian, and P. E. Arratia, *Sci. Rep.* **5**, 15761 (2015).
- [11] S. Rashid, Z. Long, S. Singh, M. Kohram, H. Vashistha, S. Navlakha, H. Salman, Z. N. Oltvai, and Z. Bar-Joseph, *Proc. Natl. Acad. Sci. USA* **116**, 11770 (2019).
- [12] G. I. Taylor, A. D. McEwan, and L. N. J. de Jong, *Proc. R. Soc. London Ser. A* **291**, 159 (1966).
- [13] J. R. Melcher and G. I. Taylor, *Annu. Rev. Fluid Mech.* **1**, 111 (1969).
- [14] J. C. Baygents and D. A. Saville, *AIP Conf. Proc.* **197**, 7 (1990).
- [15] O. Schnitzer and E. Yariv, *J. Fluid Mech.* **773**, 1 (2015).
- [16] G. A. H. Elton, *Proc. R. Soc. London Ser. A* **197**, 568 (1949).
- [17] F. Booth, *J. Chem. Phys.* **22**, 1956 (1954).
- [18] R. G. Cox, *J. Fluid Mech.* **338**, 1 (1997).
- [19] H. Ohshima, T. W. Healy, L. R. White, and R. W. O'Brien, *J. Chem. Soc. Faraday Trans. 2* **80**, 1299 (1984).
- [20] S. G. Bie and D. C. Prieve, *J. Colloid Interface Sci.* **136**, 95 (1990).

- [21] E. Yariv, O. Schnitzer, and I. Frankel, *J. Fluid Mech.* **685**, 306 (2011).
- [22] M. von Smoluchowski, in *Handbuch der Elektrizität und des Magnetismus: Stationäre Ströme*, edited by L. Graetz (Barth, Leipzig, 1921), Vol. II.
- [23] O. Schnitzer, I. Frankel, and E. Yariv, *J. Fluid Mech.* **704**, 109 (2012).
- [24] O. Schnitzer and E. Yariv, *J. Fluid Mech.* **786**, 84 (2016).
- [25] P. M. Vlahovska and R. S. Gracia, *Phys. Rev. E* **75**, 016313 (2007).
- [26] H. A. Stone and A. D. T. Samuel, *Phys. Rev. Lett.* **77**, 4102 (1996).
- [27] J. Chen, N. E. Clay, N.-h. Park, and H. Kong, *Chem. Eng. Sci. Pharm. Part. Process.* **125**, 20 (2015).
- [28] A. G. Class, B. J. Matkowsky, and A. Y. Klimenko, *J. Fluid Mech.* **491**, 11 (2003).
- [29] A. G. Class, B. J. Matkowsky, and A. Y. Klimenko, *J. Fluid Mech.* **491**, 51 (2003).
- [30] P. G. Marthaler and A. G. Class, *PAMM* **20**, 202000044 (2021).
- [31] R. Aris, *Vectors, Tensors, and the Basic Equations of Fluid Mechanics* (Dover, New York, 1989).
- [32] E. J. Hinch, *Perturbation Methods* (Cambridge University Press, Cambridge, 1991).
- [33] M. Van Dyke, *Perturbation Methods in Fluid Mechanics* (Academic, Stanford, 1964).
- [34] L. Prandtl, *Verhandlungen des III. Internationalen Mathematiker-Kongresses in Heidelberg vom 8. bis 13. August 1904* (Teubner, Leipzig, Germany, 1905), pp. 484–494.
- [35] L. Prandtl, *Z. Angew. Math. Mech.* **18**, 77 (1938).
- [36] D. Drew, L. Cheng, and R. T. Lahey, *Int. J. Multiphase Flow* **5**, 233 (1979).
- [37] O. Schnitzer and E. Yariv, *Phys. Rev. E* **86**, 021503 (2012).
- [38] M. S. Kilic, M. Z. Bazant, and A. Ajdari, *Phys. Rev. E* **75**, 021503 (2007).
- [39] M. Gouy, *J. Phys. Théor. Appl.* **9**, 457 (1910).
- [40] J. W. Gibbs, *Trans. Conn. Acad. Arts Sci.* **3**, 108 (1876).
- [41] G. G. Stokes, *Trans. Cambridge Philos. Soc.* **9**, 8 (1850).
- [42] H. Brenner, *Chem. Eng. Sci.* **19**, 703 (1964).